PROCEEDINGS OF SCIENCE

Dynamical position and orientation calibration of the KM3NeT telescope

Félix Bretaudeau,[a] **Clara Gatius Oliver,**[b,*] **Maarten de Jong**[b,c] **and Lilian Martin**[a]

[a] *Subatech, IMT Atlantique, IN2P3-CNRS, Université de Nantes,*
4 rue Alfred Kastler - La Chantrerie, Nantes, BP 20722 44307 France
[b] *Nikhef, National Institute for Subatomic Physics,*
PO Box 41882, Amsterdam, 1009 DB Netherlands
[c] *Leiden University, Leiden Institute of Physics,*
PO Box 9504, Leiden, 2300 RA Netherlands

E-mail: cgatius@km3net.de

KM3NeT is an underwater neutrino telescope which detects the Cherenkov radiation created by the products of neutrino interactions. To accurately reconstruct neutrino events, a precise determination of the position and orientation of the optical modules, which detect the Cherenkov radiation, is required. As the detector elements sway with the deep sea currents, a continuous tracking of the positions and orientations is necessary. A network of acoustic emitters and receivers is used to position the optical modules. Their orientation is determined by compasses placed in each optical module. This contribution presents the methods to perform the position and orientation calibration of the KM3NeT telescope. The positions of the optical modules need to be resolved with an accuracy of better than 20 cm in order to achieve the envisaged angular resolution of the KM3NeT/ARCA telescope of 0.05 degrees. The orientations of the optical modules need to be resolved with an accuracy of about 3 degrees in order to not compromise the quality of the event reconstruction.

38th International Cosmic Ray Conference (ICRC2023)
26 July - 3 August, 2023
Nagoya, Japan

*Speaker

PoS(ICRC2023)1033

1. Introduction

KM3NeT is an underwater neutrino telescope located at two sites in the Mediterranean sea. Neutrinos are indirectly detected by the products of their interactions in the sea water, which produce Cherenkov radiation. The ORCA[1] detector, off the coast of Toulon, is used to measure atmospheric neutrino oscillations, and the ARCA[2] detector, off the coast of Sicily, is used to search for neutrinos from astrophysical sources.

Cherenkov radiation is measured by photo-multiplier tubes (PMTs) placed in pressure-resistant glass spheres called Digital Optical Modules (DOMs). Each DOM houses 31 PMTs, the front-end and readout electronics and calibration devices, which are relevant to this work [1]. Eighteen optical modules are attached to two vertical Dyneema® ropes via a titanium collar, forming the detection units (DUs). DUs are attached to an anchor to ensure a fixed position at the sea bed, while at the top a buoy is placed to reduce its movement. Due to the different science goals of ARCA and ORCA, the detectors are build to be sensitive to higher energy (TeV-PeV) and lower energy (GeV-TeV) neutrinos, respectively. This is achieved by a different inter-DU and inter-DOM spacing, which results in about 700 m long detection units for ARCA and 200 m for ORCA [2].

To accurately reconstruct neutrino events, a precise determination of the position and orientation of the optical modules is required. However, the detection units tilt with the sea current, causing a displacement of the optical modules, and twist around their vertical axis, modifying the orientation of the PMTs. Hence, a continuous tracking of the positions and orientations of the optical modules is necessary. The optical module positions are determined by an acoustic positioning system, while their orientation is determined by compasses.

In this contribution we present the methods used to determine the fixed or static parameters in the system, as well as the dynamic position and orientation calibration of the optical modules. To achieve the envisaged angular resolution of the ARCA detector of 0.05 degrees, the positions of the optical modules need to be resolved with an accuracy of better than 20 cm, which corresponds to a hit time uncertainty of around 1 nanosecond in water. The optical modules orientation need to be resolved to an accuracy of about 3 degrees, to not compromise the event reconstruction quality [2]. The present calibration method concerns the relative positions and orientations of the optical modules, but not the absolute position and orientation of the detector. The second has to be determined with a different approach, as dedicated sea operations or studying the atmospheric muons created by cosmic rays shadowed by the Moon or Sun [3].

2. Acoustic position calibration

2.1 Acoustic positioning system

Piezo-electric acoustic sensors are housed within the optical modules and external piezo sensors are located at the base modules of the detection units. The latter are not yet used for the position calibration. The emitters are placed in autonomous tripod structures on the sea bed, on some of the anchors of the detection units and on some of the electrical junction boxes where the detection

[1] Oscillation Research with Cosmics in the Abyss
[2] Astroparticle Research with Cosmics in the Abyss

units are connected [4]. In Fig.1 the footprint of the current configuration of the ARCA and ORCA detectors are shown, indicating the location of the detection units and the emitters.

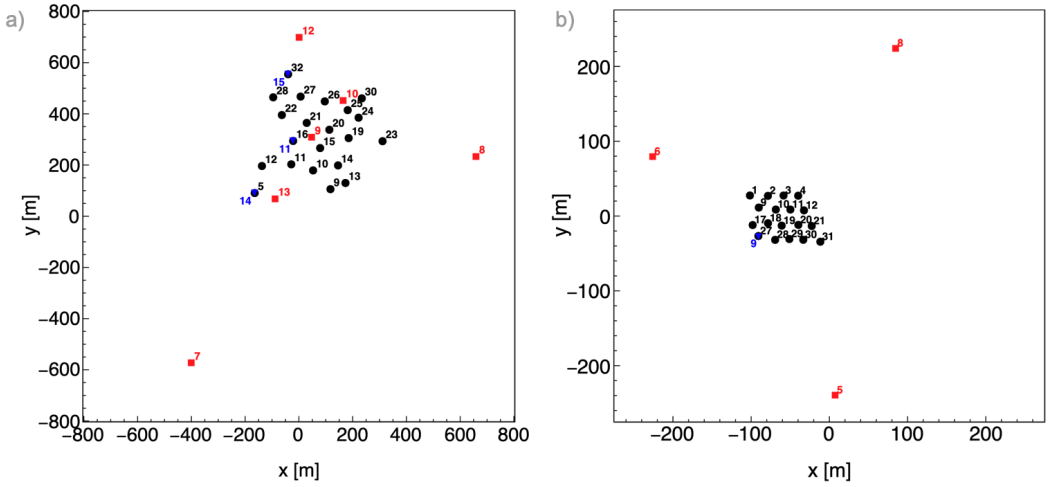

Figure 1: Footprint of the current (a) ARCA and (b) ORCA detector configurations. The x and y direction correspond to easting and northing with respect the detectors reference frame. Detection units are represented by black dots, autonomous acoustic emitters by red squares and emitters on the base modules by blue triangles.

The emitters are distributed within the detector footprint, ensuring a proper positioning of the optical modules in the horizontal plane, as well as their height. The emission pattern of the autonomous emitters, which are battery powered, is of the order of 10 consecutive emissions or pings every 10 minutes. The emitters which are connected to the base modules or junction boxes, emit continuously, approx. 1 ping every 30 seconds. Each of the emitters has an specific frequency, which is recognised by an acoustic data filter. The filter matches the corresponding waveform of the signal with the raw data, giving as output, among others, a time-of-arrival and an emitter identifier.

2.2 Acoustic fit

From each recorded time-of-arrival a preliminary estimation of the time-of-emission is computed assuming the nominal position of the optical modules that recorded the signal. If enough optical modules measure an emission within a certain time window, an acoustic event is triggered. The acoustic fit takes as input a set of acoustic events and fits a model of the detector geometry to the acoustic data. The set consists on acoustic events within a time window of 10 min, during which detector elements are assumed to not move significantly. This ensures that pings from all emitters are used for the fit.

The model describing the detector geometry is parameterised as a function of fixed or static parameters and dynamic parameters, the latter fitted every 10 min. The fixed parameters consist of the anchor position of the DUs; the height of each DOM in the DU; the piezo-sensor position in the base module, which depends on the anchor orientation; and the emitter positions on the sea bed. For the fit are also required two fixed mechanical model parameters describing the DU shape, which are computed beforehand, and the sound velocity at the detector depths, which has been measured. The dynamic parameters are 2 tilt angles and their second order corrections; a dynamical stretching

factor, which describes the creep and stretching due to the tilt, of the Dyneema® ropes holding the DU together; and the time-of-emission of each ping.

The equation relating the times of flight with the detector geometry is the following:

$$t_A^c[i,j] = t_E^c + \mid \vec{x}_0[i] + \Delta\vec{x}[i,j] - \vec{x}^c \mid v^{-1} \tag{1}$$

Where $t_A^c[i,j]$ is the time-of-arrival at DU i DOM j of emitter c, t_E^c is its time-of-emission, $\vec{x}_0[i]$ is the position of the DU anchor, $\Delta\vec{x}[i,j]$ is a vector from the anchor of the DU to DOM j [3], $\vec{x}^c$ is the position of emitter c and v is the average speed of sound in between emitter and receiver.

The vector $\Delta\vec{x}[i,j]$ is described as a function of the mechanical model of the detection unit and its tilt and stretching. The mechanical model of the detection unit describes its curvature with respect to the vertical considering the buoyancy and the drag force of all elements [5]. In the following equation the effective height, given the nominal height of the DOM z_0, the phenomenological parameters a and b describing the curvature of the DU and a stretching factor $(1+\alpha)$, is shown.

$$z' = (1+\alpha)\ z_0 + b\log(1 - a\ (1+\alpha)\ z_0) \tag{2}$$

The tilt is represented by a unit vector $\hat{T} = (T_x, T_y, (1 - T_x^2 - T_y^2)^{1/2})$, where T_x and T_y are the gradients of the x and y positions in the z' direction. The components of the $\Delta\vec{x}[i,j]$ vector in Eq.1 can be expressed in the following way:

$$\Delta x[i,j] = T_x[i]z'[i,j] + T_x^{(2)}[i](z_0[i,j])^2 \tag{3}$$

$$\Delta y[i,j] = T_y[i]z'[i,j] + T_y^{(2)}[i](z_0[i,j])^2 \tag{4}$$

$$\Delta z[i,j] = f^{-1}(\ (1+\alpha[i])z_0[i,j]\ ) \tag{5}$$

where $z'[i,j]$ is the effective height and follows Eq.2, considering the dependence of the parameters of each DOM or DU. Second order corrections of the tilt $(T_x^{(2)}, T_y^{(2)})$ are taken into account to compute the horizontal displacement of the DOMs. These are introduced to correct for possible features not taken into account by the mechanical model, for example, the effect of varying sea currents. The vector component $\Delta z[i,j]$ is obtained by computing the length of the DU, $(1+\alpha)z_0$, as a function of the height z and inverting the equation. This is computed from the horizontal displacements and effective height.

2.2.1 Minimisation method

The fit minimises the χ^2, which is the sum of differences between the measured and modelled times of arrival normalised by an assumed resolution, chosen to be 50 μs ($\sim$ 7.5 cm). Each measured time of arrival involves 6 dynamic parameters: 2 tilt angles and their second order corrections, a stretching factor and the time-of-emission. Given that a 10 min data set is used as input to the fit, the number of free parameters amounts to $n_f = \sum_{i=1}^{M} n_i + 5N$, where M is the number of emitters, n_i the number of emissions within 10 min per emitter, and N the number of DUs. The number of data points corresponds to $n_p = \sum_{i=1}^{M} n_i \cdot N \cdot 18$, where 18 is the number of optical modules in a DU. As a result, the number of degrees of freedom is very large $NDF \equiv n_p - n_f$, increasing with

[3] To ease the calculation, the third component of $\vec{x}_0[i]$ is set to 0 and the nominal height z_0 is incorporated in $\Delta\vec{x}[i,j]$.

each new emitter, receiver or detection unit. The fit uses a Lorentzian M-estimator to mitigate the effect of possible outliers.

2.2.2 Determination of the fixed parameters

The values of the fixed parameters are determined after the deployment of each new detection unit or acoustic emitter. For this, a fit of multiple fits is required, not only to determine the dynamic parameters, but also the fixed ones. The fixed parameters amount to 4 per DU (position and initial stretching), 1 per DOM (height) and 3 for each emitter (position). A set of static parameters is used to fit the dynamic ones, and a conjugate gradient method is implemented to determine the fixed parameters minimising the χ^2. The less constrained fixed parameters are varied first.

2.3 Dynamic calibration

The dynamic parameters are fitted every 10 min, updating the tilt and stretching of each DU, hence, the displacement of the optical modules. In Fig.2a and 2b, the tilt ($\hat{T}$) amplitude and orientation are shown for four months of the ORCA detector, with a configuration of six detection units. A coherent movement between the detection units is observed in both plots. In Fig.2d and 2e, the square of the sea current speed and the direction are displayed, measured at the detector location during the same period as the tilts. From the mechanical model of the detection units, the square of the sea current speed should be proportional to the tilt. As can be seen, the two quantities have a coherent behaviour, as well as the tilt orientation and sea current direction.

In Fig.3, the tilt amplitude and orientation for few days of the current ARCA detector, consisting of 21 lines, is shown. The tilt reaches values up to 100 mrad ($\sim$ 5.7 deg), highlighting the importance of the position calibration to achieve the envisaged angular resolution. The creep and dynamic stretching of the detection units is shown in Fig.4, for the period of the ARCA detector with a configuration of 6 detection units. The oldest detection unit, DU 9, shows a constant stretching, since it had already been deployed for several months, while the other detection units show a creep due to their adaptation to the medium.

In Fig.5, the residuals of the fit for one detection unit during two different periods of the ARCA detector are shown. The residual distributions in Fig.5a correspond to the period shown in Fig.3, during which extremely high tilts are fitted. The residuals expand beyond ± 100 μs ($\sim$ 15 cm), specially for the top optical modules of the detection unit. Instead, the distributions in Fig.5b correspond to a period with low tilts, and are well contained within a range of ± 100 μs.

3. Orientation calibration

3.1 Compass system

A magnetometer and accelerometer are integrated in each optical module, referred to as "compass", which can provide the yaw, pitch and roll of the module [1]. The compass data is continuously recorded every 10 sec and calibrated with in-lab compass measurements. To convert the calibrated data to yaw, pitch and roll, a correction for the magnetic declination and the meridian convergence angle needs to be applied, which is different in the two sites of the detector. The compass data is converted to quaternions, which are a compact way to describe rotations: $Q \equiv (\cos(\theta/2), \sin(\theta/2)\hat{u})$, where θ is the rotation angle around the axis $\hat{u}$.

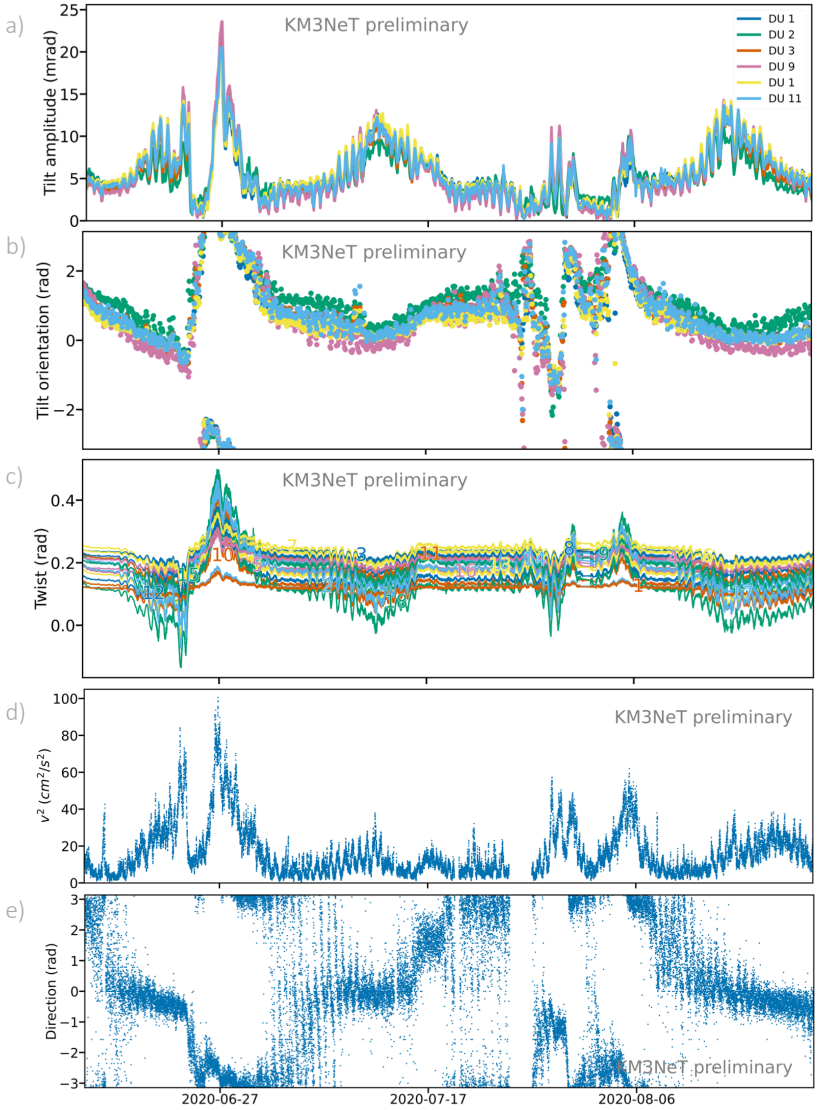

Figure 2: (a) Tilt amplitude for each detection unit. (b) Tilt orientation for each detection unit. (c) Twist of the optical modules from detection unit 11. The different modules are indicated by a number corresponding to their position along the DU; 1 for the lowest module, 18 for the top one. (d) Square of the measured sea current velocity. (e) Measured sea current direction. All plots are for the same period, which comprises four months of the ORCA detector with a configuration of six detection units.

3.2 Static calibration

An *in-situ* calibration of the optical module orientations is done, which consists of the alignment of the modules for each detection unit. This is applied by fitting the compass data within a time window of 10 min, to a model of the DU twist around the vertical axis. The model is a polynomial function, where Q_0 represents the tilt of the DU and Q_1 represents its twist around the vertical axis, which depends on the height of each module z_i. The model ensures a continuous change of the twist along the DU.

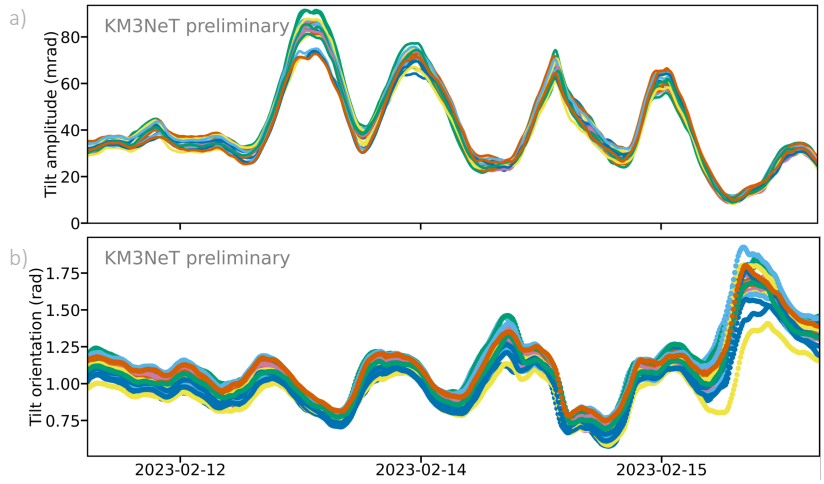

Figure 3: a) Tilt amplitude and b) tilt orientation, for a few days period of the current ARCA detector, with a 21 detection units configuration. The different lines indicate different detection units.

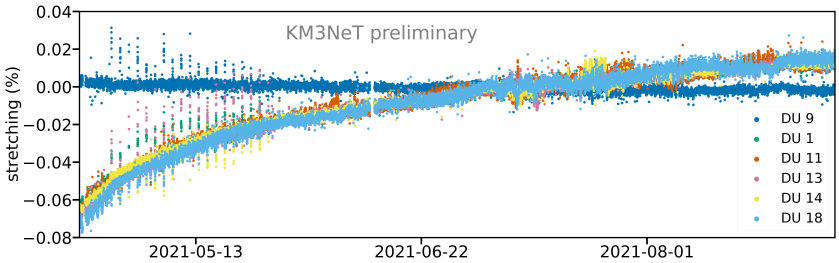

Figure 4: Stretching as a function of time for the ARCA detector, during the period it had a 6 detection units configuration.

$$Q = Q_0\, Q_1^{z_i} \tag{6}$$

Multiple fits are performed during a period in which the DUs do not move significantly. The fit minimises the χ^2, defined as the square of the shortest angle between the measured and modelled quaternion of the DOMs within a DU, normalised by an assumed resolution of 1 deg. The average residual between the modelled and measured quaternion constitutes the alignment of the DOM.

3.3 Dynamic calibration

The orientation of the optical modules are updated every 5 min, using the continuous recording of compass data. After applying the lab calibration and the alignment of the compasses, the data is filtered by removing measurements that deviate more than 5 deg from a local interpolation of the time-ordered data. In case a DOM does not record data, an interpolation with the neighbouring DOMs measurements is applied to find its orientation. In Fig.2 the dynamic orientation of the DOMs of the detection unit 11, during four months of the ORCA detector with a configuration of six detection units, is shown. The DOMs move coherently among themselves as well as with the tilt amplitude and orientation variations derived from the acoustic data.

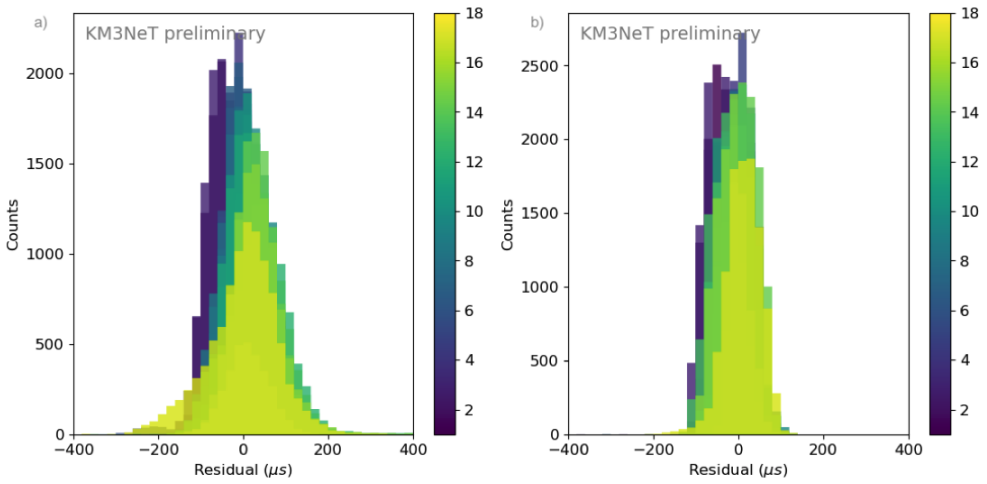

Figure 5: a) Residuals of the fit for a detection unit of the current ARCA detector, during the period shown in Fig. 3. b) Residuals during a period with small values of the tilt. The colour scheme indicates the floor of the modules; 1 for the lowest module, 18 for the top one.

4. Conclusion

Acoustic positioning and orientation methods are developed to calibrate the static and dynamic positions and orientations of the optical modules. These are cross-checked by a muon calibration technique, which exploits the muon track reconstruction to find the optimal orientation, position and time reference of the optical modules. The positions are found to agree with the muon calibration within a range of ±10 cm while the orientations show an agreement within a range of less than ±3 deg [6]. The agreement is within the required specifications to achieve the envisaged angular resolution of the KM3NeT telescope.

References

[1] S. Aiello et al. The KM3NeT multi-PMT digital optical module. *J. Inst.*, 17, 2022.

[2] S. Adrián-Martínez et al. Letter of intent for KM3NeT 2.0. *Journal of Physics G: Nuclear and Particle Physics*, 43(8), 2016.

[3] S. Aiello et al. First observation of the cosmic ray shadow of the Moon and the Sun with KM3NeT/ORCA. *Eur. Phys. J. C*, 83(4), 2023.

[4] S. Viola et al. Acoustic positioning system for KM3NeT. *PoS ICRC2015*, 236, 2015.

[5] Dídac D. Tortosa. Monitoring and reconstruction of the shape of the Detection Units in KM3NeT using acoustic and compass sensors. *Sensors (Switzerland)*, 20(18), 2020.

[6] Louis Bailly-Salins. Time, position and orientation calibration using atmospheric muons in KM3NeT. *PoS ICRC2023*, 218, 2023.

Full Authors List: The KM3NeT Collaboration

S. Aiello[a], A. Albert[b,bd], S. Alves Garre[c], Z. Aly[d], A. Ambrosone[f,e], F. Ameli[g], M. Andre[h], E. Androutsou[i], M. Anguita[j], L. Aphecetche[k], M. Ardid[l], S. Ardid[l], H. Atmani[m], J. Aublin[n], L. Bailly-Salins[o], Z. Bardačová[q,p], B. Baret[n], A. Bariego-Quintana[c], S. Basegmez du Pree[r], Y. Becherini[n], M. Bendahman[m,n], F. Benfenati[t,s], M. Benhassi[u,e], D. M. Benoit[v], E. Berbee[r], V. Bertin[d], S. Biagi[w], M. Boettcher[x], D. Bonanno[w], J. Boumaaza[m], M. Bouta[y], M. Bouwhuis[r], C. Bozza[z,e], R. M. Bozza[f,e], H.Brânzaş[aa], F. Bretaudeau[k], R. Bruijn[ab,r], J. Brunner[d], R. Bruno[a], E. Buis[ac,r], R. Buompane[u,e], J. Busto[d], B. Caiffi[ad], D. Calvo[c], S. Campion[g,ae], A. Capone[g,ae], F. Carenini[t,s], V. Carretero[c], T. Cartraud[n], P. Castaldi[af,s], V. Cecchini[c], S. Celli[g,ae], L. Cerisy[d], M. Chabab[ag], M. Chadolias[ah], A. Chen[ai], S. Cherubini[aj,w], T. Chiarusi[s], M. Circella[ak], R. Cocimano[w], J. A. B. Coelho[n], A. Coleiro[n], R. Coniglione[w] P. Coyle[d], A. Creusot[n], A. Cruz[al], G. Cuttone[w], R. Dallier[k], Y. Darras[ah], A. De Benedittis[e], B. De Martino[d], V. Decoene[k], R. Del Burgo[e], U. M. Di Cerbo[e], L. S. Di Mauro[w], I. Di Palma[g,ae], A. F. Díaz[j], C. Diaz[j], D. Diego-Tortosa[w], C. Distefano[w], A. Domi[ah], C. Donzaud[n], D. Dornic[d], M. Dörr[am], E. Drakopoulou[i], D. Drouhin[b,bd], R. Dvornický[q], T. Eberl[ah], E. Eckerová[q,p], A. Eddymaoui[m], T. van Eeden[r], M. Eff[n], D. van Eijk[r], I. El Bojaddaini[y], S. El Hedri[n], A. Enzenhöfer[d], G. Ferrara[w], M. D. Filipović[an], F. Filippini[t,s], D. Franciotti[w], L. A. Fusco[z,e], J. Gabriel[ao], S. Gagliardini[g], T. Gal[ah], J. García Méndez[l], A. Garcia Soto[c], C. Gatius Oliver[r], N. Geißelbrecht[ah], H. Ghaddari[y], L. Gialanella[e,u], B. K. Gibson[v], E. Giorgio[w], I. Goos[n], D. Goupilliere[o], S. R. Gozzini[c], R. Gracia[ah], K. Graf[ah], C. Guidi[ap,ad], B. Guillon[o], M. Gutiérrez[aq], H. van Haren[ar], A. Heijboer[r], A. Hekalo[am], L. Hennig[ah], J. J. Hernández-Rey[c], F. Huang[d], W. Idrissi Ibnsalih[e], G. Illuminati[s], C. W. James[al], M. de Jong[as,r], P. de Jong[ab,r], B. J. Jung[r], P. Kalaczyński[at,be], O. Kalekin[ah], U. F. Katz[ah], N. R. Khan Chowdhury[c], A. Khatun[q], G. Kistauri[av,au], C. Kopper[ah], A. Kouchner[aw,n], V. Kulikovskiy[ad], R. Kvatadze[av], M. Labalme[o], R. Lahmann[ah], G. Larosa[w], C. Lastoria[d], A. Lazo[c], S. Le Stum[d], G. Lehaut[o], E. Leonora[a], N. Lessing[c], G. Levi[t,s], M. Lindsey Clark[n], F. Longhitano[a], J. Majumdar[r], L. Malerba[ad], F. Mamedov[p], J. Mańczak[c], A. Manfreda[e], M. Marconi[ap,ad], A. Margiotta[t,s], A. Marinelli[e,f], C. Markou[i], L. Martin[k], J. A. Martínez-Mora[l], F. Marzaioli[u,e], M. Mastrodicasa[ae,g], S. Mastroianni[e], S. Miccichè[w], G. Miele[f,e], P. Migliozzi[e], E. Migneco[w], M. L. Mitsou[e], C. M. Mollo[e], L. Morales-Gallegos[u,e], C. Morley-Wong[al], A. Moussa[y], I. Mozun Mateo[ay,ax], R. Muller[r], M. R. Musone[e,u], M. Musumeci[w], L. Nauta[r], S. Navas[aq], A. Nayerhoda[ak], C. A. Nicolau[g], B. Nkosi[ai], B. Ó Fearraigh[ab,r], V. Oliviero[f,e], A. Orlando[w], E. Oukacha[n], D. Paesani[w], J. Palacios González[c], G. Papalashvili[au], V. Parisi[ap,ad], E.J. Pastor Gomez[c], A. M. Păun[aa], G. E. Păvălaş[aa], S. Peña Martínez[n], M. Perrin-Terrin[d], J. Perronnel[o], V. Pestel[ay], R. Pestes[n], P. Piattelli[w], C. Poirè[z,e], V. Popa[aa], T. Pradier[b], S. Pulvirenti[w], G. Quéméner[o], C. Quiroz[l], U. Rahaman[c], N. Randazzo[a], R. Randriatoamanana[k], S. Razzaque[az], I. C. Rea[e], D. Real[c], S. Reck[ah], G. Riccobene[w], J. Robinson[x], A. Romanov[ap,ad], A. Šaina[c], F. Salesa Greus[c], D. F. E. Samtleben[as,r], A. Sánchez Losa[c,ak], S. Sanfilippo[w], M. Sanguineti[ap,ad], C. Santonastaso[ba,e], D. Santonocito[w], P. Sapienza[w], J. Schnabel[ah], J. Schumann[ah], H. M. Schutte[x], J. Seneca[r], N. Sennan[y], B. Setter[ah], I. Sgura[ak], R. Shanidze[au], Y. Shitov[p], F. Šimkovic[q], A. Simonelli[e], A. Sinopoulou[a], M.V. Smirnov[ah], B. Spisso[e], M. Spurio[t,s], D. Stavropoulos[i], I. Štekl[p], M. Taiuti[ap,ad], Y. Tayalati[m], H. Tedjditi[ad], H. Thiersen[x], I. Tosta e Melo[a,aj], B. Trocmé[n], V. Tsourapis[i], E. Tzamariudaki[i], A. Vacheret[o], V. Valsecchi[w], V. Van Elewyck[aw,n], G. Vannoye[d], G. Vasileiadis[bb], F. Vazquez de Sola[r], C. Verilhac[n], A. Veutro[g,ae], S. Viola[w], D. Vivolo[u,e], J. Wilms[bc], E. de Wolf[ab,r], H. Yepes-Ramirez[l], G. Zarpapis[i], S. Zavatarelli[ad], A. Zegarelli[g,ae], D. Zito[w], J. D. Zornoza[c], J. Zúñiga[c], and N. Zywucka[x].

[a] INFN, Sezione di Catania, Via Santa Sofia 64, Catania, 95123 Italy
[b] Université de Strasbourg, CNRS, IPHC UMR 7178, F-67000 Strasbourg, France
[c] IFIC - Instituto de Física Corpuscular (CSIC - Universitat de València), c/Catedrático José Beltrán, 2, 46980 Paterna, Valencia, Spain
[d] Aix Marseille Univ, CNRS/IN2P3, CPPM, Marseille, France
[e] INFN, Sezione di Napoli, Complesso Universitario di Monte S. Angelo, Via Cintia ed. G, Napoli, 80126 Italy
[f] Università di Napoli "Federico II", Dip. Scienze Fisiche "E. Pancini", Complesso Universitario di Monte S. Angelo, Via Cintia ed. G, Napoli, 80126 Italy
[g] INFN, Sezione di Roma, Piazzale Aldo Moro 2, Roma, 00185 Italy
[h] Universitat Politècnica de Catalunya, Laboratori d'Aplicacions Bioacústiques, Centre Tecnològic de Vilanova i la Geltrú, Avda. Rambla Exposició, s/n, Vilanova i la Geltrú, 08800 Spain
[i] NCSR Demokritos, Institute of Nuclear and Particle Physics, Ag. Paraskevi Attikis, Athens, 15310 Greece
[j] University of Granada, Dept. of Computer Architecture and Technology/CITIC, 18071 Granada, Spain
[k] Subatech, IMT Atlantique, IN2P3-CNRS, Université de Nantes, 4 rue Alfred Kastler - La Chantrerie, Nantes, BP 20722 44307 France
[l] Universitat Politècnica de València, Instituto de Investigación para la Gestión Integrada de las Zonas Costeras, C/ Paranimf, 1, Gandia, 46730 Spain
[m] University Mohammed V in Rabat, Faculty of Sciences, 4 av. Ibn Battouta, B.P. 1014, R.P. 10000 Rabat, Morocco
[n] Université Paris Cité, CNRS, Astroparticule et Cosmologie, F-75013 Paris, France
[o] LPC CAEN, Normandie Univ, ENSICAEN, UNICAEN, CNRS/IN2P3, 6 boulevard Maréchal Juin, Caen, 14050 France
[p] Czech Technical University in Prague, Institute of Experimental and Applied Physics, Husova 240/5, Prague, 110 00 Czech Republic
[q] Comenius University in Bratislava, Department of Nuclear Physics and Biophysics, Mlynska dolina F1, Bratislava, 842 48 Slovak Republic
[r] Nikhef, National Institute for Subatomic Physics, PO Box 41882, Amsterdam, 1009 DB Netherlands
[s] INFN, Sezione di Bologna, v.le C. Berti-Pichat, 6/2, Bologna, 40127 Italy
[t] Università di Bologna, Dipartimento di Fisica e Astronomia, v.le C. Berti-Pichat, 6/2, Bologna, 40127 Italy
[u] Università degli Studi della Campania "Luigi Vanvitelli", Dipartimento di Matematica e Fisica, viale Lincoln 5, Caserta, 81100 Italy
[v] E. A. Milne Centre for Astrophysics, University of Hull, Hull, HU6 7RX, United Kingdom

[w] INFN, Laboratori Nazionali del Sud, Via S. Sofia 62, Catania, 95123 Italy
[x] North-West University, Centre for Space Research, Private Bag X6001, Potchefstroom, 2520 South Africa
[y] University Mohammed I, Faculty of Sciences, BV Mohammed VI, B.P. 717, R.P. 60000 Oujda, Morocco
[z] Università di Salerno e INFN Gruppo Collegato di Salerno, Dipartimento di Fisica, Via Giovanni Paolo II 132, Fisciano, 84084 Italy
[aa] ISS, Atomistilor 409, Măgurele, RO-077125 Romania
[ab] University of Amsterdam, Institute of Physics/IHEF, PO Box 94216, Amsterdam, 1090 GE Netherlands
[ac] TNO, Technical Sciences, PO Box 155, Delft, 2600 AD Netherlands
[ad] INFN, Sezione di Genova, Via Dodecaneso 33, Genova, 16146 Italy
[ae] Università La Sapienza, Dipartimento di Fisica, Piazzale Aldo Moro 2, Roma, 00185 Italy
[af] Università di Bologna, Dipartimento di Ingegneria dell'Energia Elettrica e dell'Informazione "Guglielmo Marconi", Via dell'Università 50, Cesena, 47521 Italia
[ag] Cadi Ayyad University, Physics Department, Faculty of Science Semlalia, Av. My Abdellah, P.O.B. 2390, Marrakech, 40000 Morocco
[ah] Friedrich-Alexander-Universität Erlangen-Nürnberg (FAU), Erlangen Centre for Astroparticle Physics, Nikolaus-Fiebiger-Straße 2, 91058 Erlangen, Germany
[ai] University of the Witwatersrand, School of Physics, Private Bag 3, Johannesburg, Wits 2050 South Africa
[aj] Università di Catania, Dipartimento di Fisica e Astronomia "Ettore Majorana", Via Santa Sofia 64, Catania, 95123 Italy
[ak] INFN, Sezione di Bari, via Orabona, 4, Bari, 70125 Italy
[al] International Centre for Radio Astronomy Research, Curtin University, Bentley, WA 6102, Australia
[am] University Würzburg, Emil-Fischer-Straße 31, Würzburg, 97074 Germany
[an] Western Sydney University, School of Computing, Engineering and Mathematics, Locked Bag 1797, Penrith, NSW 2751 Australia
[ao] IN2P3, LPC, Campus des Cézeaux 24, avenue des Landais BP 80026, Aubière Cedex, 63171 France
[ap] Università di Genova, Via Dodecaneso 33, Genova, 16146 Italy
[aq] University of Granada, Dpto. de Física Teórica y del Cosmos & C.A.F.P.E., 18071 Granada, Spain
[ar] NIOZ (Royal Netherlands Institute for Sea Research), PO Box 59, Den Burg, Texel, 1790 AB, the Netherlands
[as] Leiden University, Leiden Institute of Physics, PO Box 9504, Leiden, 2300 RA Netherlands
[at] National Centre for Nuclear Research, 02-093 Warsaw, Poland
[au] Tbilisi State University, Department of Physics, 3, Chavchavadze Ave., Tbilisi, 0179 Georgia
[av] The University of Georgia, Institute of Physics, Kostava str. 77, Tbilisi, 0171 Georgia
[aw] Institut Universitaire de France, 1 rue Descartes, Paris, 75005 France
[ax] IN2P3, 3, Rue Michel-Ange, Paris 16, 75794 France
[ay] LPC, Campus des Cézeaux 24, avenue des Landais BP 80026, Aubière Cedex, 63171 France
[az] University of Johannesburg, Department Physics, PO Box 524, Auckland Park, 2006 South Africa
[ba] Università degli Studi della Campania "Luigi Vanvitelli", CAPACITY, Laboratorio CIRCE - Dip. Di Matematica e Fisica - Viale Carlo III di Borbone 153, San Nicola La Strada, 81020 Italy
[bb] Laboratoire Univers et Particules de Montpellier, Place Eugène Bataillon - CC 72, Montpellier Cédex 05, 34095 France
[bc] Friedrich-Alexander-Universität Erlangen-Nürnberg (FAU), Remeis Sternwarte, Sternwartstraße 7, 96049 Bamberg, Germany
[bd] Université de Haute Alsace, rue des Frères Lumière, 68093 Mulhouse Cedex, France
[be] AstroCeNT, Nicolaus Copernicus Astronomical Center, Polish Academy of Sciences, Rektorska 4, Warsaw, 00-614 Poland

Acknowledgements

The authors acknowledge the financial support of the funding agencies: Agence Nationale de la Recherche (contract ANR-15-CE31-0020), Centre National de la Recherche Scientifique (CNRS), Commission Européenne (FEDER fund and Marie Curie Program), LabEx UnivEarthS (ANR-10-LABX-0023 and ANR-18-IDEX-0001), Paris Île-de-France Region, France; Shota Rustaveli National Science Foundation of Georgia (SRNSFG, FR-22-13708), Georgia; The General Secretariat of Research and Innovation (GSRI), Greece Istituto Nazionale di Fisica Nucleare (INFN), Ministero dell'Università e della Ricerca (MIUR), PRIN 2017 program (Grant NAT-NET 2017W4HA7S) Italy; Ministry of Higher Education, Scientific Research and Innovation, Morocco, and the Arab Fund for Economic and Social Development, Kuwait; Nederlandse organisatie voor Wetenschappelijk Onderzoek (NWO), the Netherlands; The National Science Centre, Poland (2021/41/N/ST2/01177); The grant "AstroCeNT: Particle Astrophysics Science and Technology Centre", carried out within the International Research Agendas programme of the Foundation for Polish Science financed by the European Union under the European Regional Development Fund; National Authority for Scientific Research (ANCS), Romania; Grants PID2021-124591NB-C41, -C42, -C43 funded by MCIN/AEI/ 10.13039/501100011033 and, as appropriate, by "ERDF A way of making Europe", by the "European Union" or by the "European Union NextGenerationEU/PRTR", Programa de Planes Complementarios I+D+I (refs. ASFAE/2022/023, ASFAE/2022/014), Programa Prometeo (PROMETEO/2020/019) and GenT (refs. CIDEGENT/2018/034, /2019/043, /2020/049. /2021/23) of the Generalitat Valenciana, Junta de Andalucía (ref. SOMM17/6104/UGR, P18-FR-5057), EU: MSC program (ref. 101025085), Programa María Zambrano (Spanish Ministry of Universities, funded by the European Union, NextGenerationEU), Spain; The European Union's Horizon 2020 Research and Innovation Programme (ChETEC-INFRA - Project no. 101008324).